Asian Journal of Chemistry; Vol. 34, No. 12 (2022), 3313-3319

ASIAN JOURNAL OF CHEMISTRY

https://doi.org/10.14233/ajchem.2022.23985

Synthesis, Characterization and Antimicrobial Activity of Nanochitosan and Chitosan Encapsulated Zinc Oxide Nanoparticles

SIVANTHAPERUMAL*, RAZIYA TABASSUM and THAMINUM ANSARI

PG & Research Department of Chemistry, Muthurangam Governmnets Arts College, Vellore-632002, India

*Corresponding author: E-mail: emiratessiva@gmail.com

Received: 29 June 2022; *Accepted*: 20 October 2022; *Published online*: 25 November 2022; AJC-21062

In recent years, nanochitosan and chitosan encapsulated zinc oxide nanoparticles have gained tremendous attention related to their unique properties such as exhibit antimicrobial properties. In this article, synthesis of nanochitosan, chitosan encapsulated zinc oxide and compared their potential applications as an antimicrobial agents were discussed. The nanochitosan and chitosan encapsulated zinc oxide nanoparticles have been characterized by ultraviolet-visible spectroscopy (UV), Fourier transform infrared spectroscopy (FT-IR), X-ray diffraction (XRD), scanning electron microscopy (SEM) techniques.

Keywords: Nanochitosan, Nanoparticles, Zinc oxide, Encapsulated, Antimicrobial activity.

INTRODUCTION

In recent years, infectious diseases, specifically those that are caused by microorganism have seen a dramatic proliferation due to resistance to multiple antibiotics, opening the colony by opportunistic pathogens. Nanotechnology has been applied in the development of new antimicrobial therapies, capable of fighting infections caused by pathogens [1]. Nanochitosan and its derivatives are widely explored as functional materials since it has good properties such as biocompatibility, biodegradability and non-toxicity and have wide variety of applications in the development of bioadhesives, nanomaterials, improved drug delivery systems [2], enteric coatings [3] and in medical devices [4,5].

Nanoparticles based metal oxide properties such as shape, size, roughness and their large surface area, make oxides ideal candidates to interact with bacteria and able to have an antimicrobial effectiveness [6]. Nanosize inorganic compounds have shown remarkable antibacterial activity at very low concentration due to their high surface area to volume ratio and unique chemical and physical features [7]. In addition, these particles are also more stable at high temperature and pressure [8]. It is known that zinc oxide nanoparticles acted as antibacterial and inhibit the growth of microorganisms by permeating into the cell membrane [9]. The oxidative stress damages lipids, carbohydrates, proteins and DNA [10]. Lipid peroxidation is obviously the most crucial that leads to alteration in cell membrane which eventually disrupt vital cellular functions [11]. It has been supported by oxidative stress mechanism involving zinc oxide nanoparticle against *Escherichia coli* [12].

Globally, bacterial infections are recognized as serious health issue. New bacterial mutation, antibiotic resistance, outbreaks of pathogenic strains, *etc.* are increasing and thus, development of more efficient antibacterial agents is demand of the time. Zinc oxide is known for its antibacterial properties from the time immemorial [13]. In past, antibacterial activity of zinc oxide nanoparticle has been investigated against four known Gram-positive and Gram-negative bacteria, namely *Staphylococcus aureus*, *Escherichia coli*, *Salmonella typhimurium* and *Klebsiella pneumoniae*. It was observed that the growth inhibiting dose of zinc oxide nanoparticles was 15 µg/mL, although in case of *K. pneumoniae*, it was as low as 5 µg/mL [14,15].

The synthesis of chitosan capped inorganic nanomaterials have been considered as significant antibacterial materials in the clinical field. The results suggested that the synthesized materials can be used in wound dressing applications was reported [16]. Polymer coated metal oxide nanoparticles are cluster of many nanocrystals within a polymer matrix [17]. The

bandage collected of composite chitosan hydrogel and ZnO nanoparticles were synthesized and their antimicrobial activity indicates that this bandage had strong effects on *E. coli* and *S. aureus*, with a highly developed antimicrobial impact on *E. coli* [18].

Production and optimization of chitosan nanoparticles encapsulated with L-ascorbic acid and thymoquinone is also reported [19]. The chitosan-copper oxide biopolymer nanocomposites were synthesized and showed significant antimicrobial activity against *Bacillus subtilis*, *Escherichia coli*, *Penicillium notatum* and *Pseudomonas aeruginosa*, assayed using the agar well diffusion method [20]. In this study, chemically modify chitosan into nanochitosan was done by using ionotropic gelation method and chitosan encapsulated zinc oxide nanoparticles is onto the backbone of nanochitosan. They were characterized by UV, FTIR, TGA, XRD and SEM which elucidated the structural changes in comparison with nanochitosan and regarding chitosan encapsulated zinc oxide nanoparticles as antibacterial and antifungal agents.

EXPERIMENTAL

Chitosan was obtained from Indian sea foods, Cochin, India. Sodium tripolyphosphate, zinc oxide, acetic acid and all other chemicals used in the experiments were of analytical grade purchased from Merck, India.

Preparation of nanochitosan: The nanochitosan was prepared by ionotropic gelation method [21] using sodium tripolyphosphate. About 1 g of chitosan was dissolved in 200 mL of 2% acetic acid solution, which was prepared using the conductivity water. The above solution was stirred well for 15 min. Then to the above prepared chitosan solution and 0.8 g of sodium tripolyphosphate dissolved in 107 mL of conductivity water. The conductivity water was added dropwise upto a milky coloured emulsion like appearance was obtained. This solution was then allowed to settle as suspension by adding conductivity water in excess for 24 h. After this process, the supersaturated solution was then decanted. The thick emulsion which was obtained above was then poured into the Petri plates.

Preparation of chitosan encapsulated ZnO nanoparticles: About 1 g of chitosan was dissolved in 200 mL of 2% acetic acid solution, which was prepared using conductivity water. The above solution was stirred well for 15 min followed by the addition of 1 g of ZnO and again stirred well. Then to the above prepared chitosan solution and 0.8 g of sodium tripolyphosphate dissolved in 107 mL of conductivity water was added. The conductivity water was added dropwise to obtain a milky coloured emulsion. This solution was then allowed to settle as suspension by adding conductivity water in excess for 24 h. After this process, the supersaturated solution was decanted. The obtained thick emulsion was then poured into the Petri plates [22].

UV-visible analysis: The absorption spectra of the synthesized nanochitosan, chitosan encapsulated zinc oxide nanoparticles were characterized by UV-visible spectroscopy using a double beam spectrophotometer. The ultraviolet-visible spectrum was recorded on Hitachi, Model U-2800 spectrophotometer using acetic acid as a solvent and equipped with a diffuse reflectance attachment for powder samples in between a wavelength scan of 200 and 800 nm.

FT-IR analysis: The synthesized nanochitosan, chitosan encapsulated zinc oxide nanoparticles were characterized by using FTIR Thermo Nicolet AVATAR 330 spectrophotometer in the range of 4000-400 cm^{-1} wavelength using KBr pellet. The FTIR spectra were normalized and major vibration bands were identified associated with surface functional groups.

Thermal analysis: Thermogravimetric analysis was performed to find the relation between weight loss of synthesized nanochitosan, chitosan encapsulated ZnO nanoparticles with increasing temperature on a SDT Q600 V 20.9 Build 20 instrument with a heating rate of 20 ºC/min in N_2 atmosphere. The weight loss at different stages and the cause for each loss was analyzed.

XRD analysis: The crystalline structure and the average crystalline size of synthesized nanochitosan, chitosan encapsulated ZnO nanoparticles were characterized using X-ray powder diffractometer (Shimadzu XD-D1) using a Ni-filtered Cu$K\alpha$ X-ray radiation source. The Debye-Scherrer's equation was used to determine the particle size of the samples from 2θ values, which is represented as:

$$D = \frac{k\lambda}{\beta\cos\theta}$$

where k = Scherrer's constant (shape factor), ranges from 0.9 to 1.0, λ = wavelength (1.541 nm) of the X-ray radiation source, β = full width half maximum of the XRD peak (radians) and θ = Bragg's angle.

SEM analysis: To analyze the morphology, average size and composition, synthesized nanochitosan, chitosan encapsulated ZnO nanoparticles was characterized by different magnification levels scanning electron microscope analysis using VEGA3 TESCAN SEM machine.

Antimicrobial studies: The nanochitosan, chitosan encapsulated zinc oxide nanoparticles were tested for their antimicrobial activity by agar well diffusion method against different pathogenic microorganisms. Three bacterial strains and two fungal strains were used for antimicrobial activity. Two Gram-negative bacteria (*E. coli* and *Salmonella typhi*) and one Gram-positive bacteria (*Staphylococcus aureus*) were tested. The fungal strains *viz. Aspergillus niger* and *Aspergillus flavus* were tested by agar well diffusion method according to the reported procedure [22].

Antibacterial studies: The sterilized medium was poured into a petri dish in a uniform thickness and kept a side for solidification. Using sterilized swabs, even distribution of lawn culture was prepared using test bacteria such as *Escherichia coli*, *Staphylococcus aureus* and *Salmonella typhi* in Muller Hinton agar (MHA) plates. Muller Hinton Agar was prepared and sterilized and then 20 mL of media was poured in Petri plates and allowed for solidification. The bacterial lawn culture was made using sterile cotton swab and labeled. The wells were made in the media with the help of a metallic borer with centers at least 24 mm. Recommended concentration 10^{-3} M of test nanochitosan, chitosan encapsulated ZnO nanoparticles

in acetic acid were introduced in the respective wells. Other wells were supplemented with reference antibacterial drug.

Antifungal assay: The antifungal activities of nanochitosan and chitosan encapsulated ZnO nanoparticles were studied against two fungal cultures, *Aspergillus niger* and *Aspergillus flavus*. Sabouraud dextrose agar was prepared, sterilized and prepare the culture plates same like Muller Hinton Agar. After solidification of media, respective fungal spore suspensions were transferred to Petri plates. The wells were made in the media with the help of sterile metallic borer with centers at least 24 mm. Recommended concentration 10^{-3} M of nanochitosan, nanochitosan, nanochitosan encapsulated ZnO and chitosan encapsulated ZnO nanoparticles in acetic acid were introduced in the respective wells. The plates were incubated immediately at 72 h. The results were recorded as zones of complete inhibition (mm). Growth inhibition was compared with standard antibiotic amphotericin B used as positive control.

RESULTS AND DISCUSSION

UV-vis spectra: The UV-vis absorbance spectra of nanochitosan and chitosan encapsulated ZnO nanoparticles are shown in Fig. 1a-b. As observed, chitosan sample did not show much absorbance in the wavelength range from 200 nm to 800 nm due to lack of conjugated double bonds in the structure [23]. Broad absorption bands observed at 200 and 322 nm could be related to the CO group [24]. In nanochitosan and chitosan encapsulated ZnO nanoparticles, the peak observed at 280 nm correspond to the interactions between nanochitosan and ZnO nanoparticles.

FT-IR spectra: The FT-IR spectra of nanochitosan was obtained from chitosan by ionotropic gelation method showed some different bands (Fig. 2a). It is remarkable that in case of nanochitosan, a strong peak was obtained at 3236.55, 2864.29, 1631.78, 1143.79 and 1064.71 cm^{-1} which indicates the presence of intermolecular hydrogen bonded NH stret-ching, asymmetrical and symmetrical CH stretching in NH_3^+, C=O stretching, OH of (O=P-OH) P=O stretching and P-O stretching and C-O-C linkage and 896.90 cm^{-1} indicate the presence of –NH bending, respectively [25].

The shift of the peak observed at 3454.75 cm^{-1} corresponding to the presence of NH, OH stretching in chitosan to lower wavenumber (3236.55 cm^{-1}) in nanochitosan samples may indicate an interaction of sodium tripolyphosphate with pure chitosan. The above observed results (Table-1) showed that the $CONH_2$ and NH_2 groups of chitosan are both slightly cross-linked with sodium polyphosphate molecule. Additionally, when compared to pure chitosan, some additional peaks in nanochitosan also appear, concluded that the nanochitosan was formed from the pure chitosan.

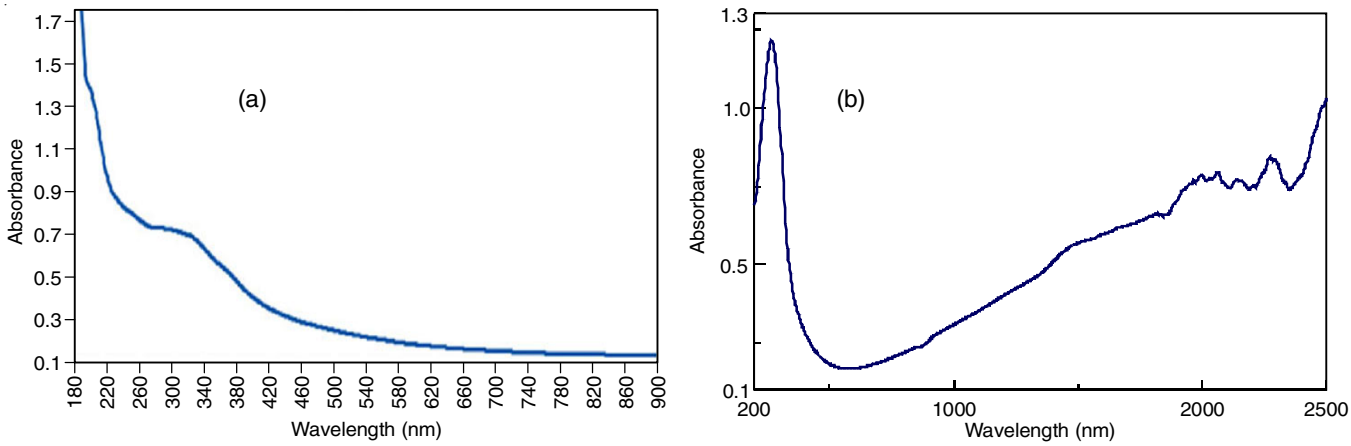

Fig. 1. UV Spectra of (a) nanochitosan and (b) chitosan encapsulated ZnO nanoparticles

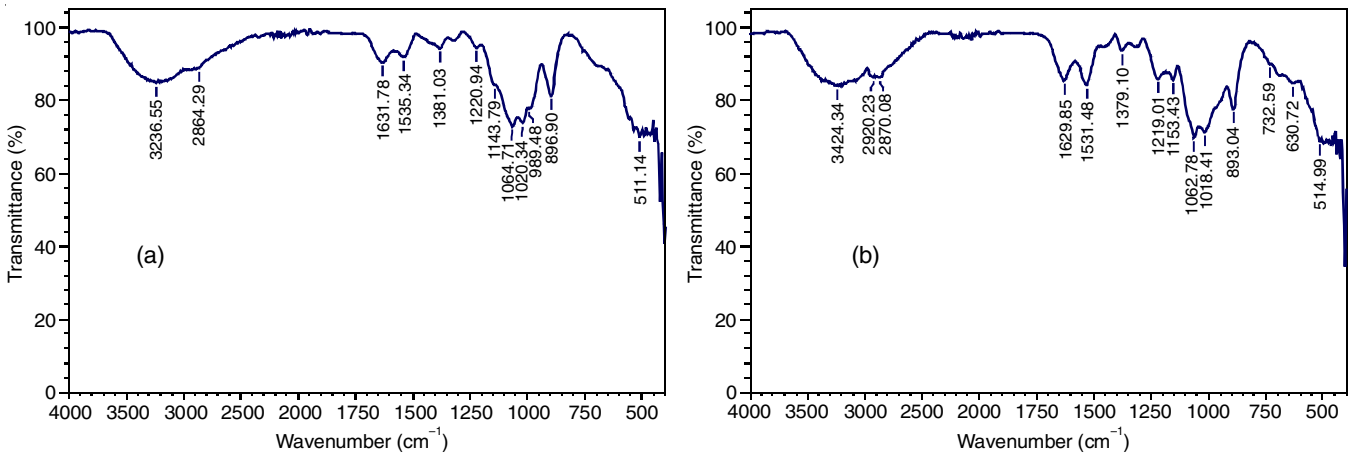

Fig. 2. FT-IR spectra of (a) nanochitosan and (b) chitosan encapsulated ZnO nanoparticles

TABLE-1
FT-IR SPECTRAL (ν, cm^{-1}) DETAILS OF NANOCHITOSAN ENCAPSULATED ZINC OXIDE AND CHITOSAN ENCAPSULATED ZINC OXIDE NANOPARTICLES

Samples	H bond N-H and OH *str.*	CH *str.*	C=O in amide	P=O *str.*	C-O-C linkage	N-H bending	ZnO
Nano chitosan	3236.55	2864.29	1631.78	1143.79	1064.71	896.90	–
Chitosan + ZnO NP's	3242.34	2920.23	1629.85	1219.01	1062.78	893.04	630.72

The IR spectrum of chitosan encapsulated ZnO nanoparticles showed a prominent peak at 3242.34 cm^{-1} corresponds to –OH stretching of axial OH group and –NH stretching (Fig. 2b). A peak at 2920.23 cm^{-1} was due to aliphatic –CH asymmetric stretching, strong peak obtained at 1629.85 cm^{-1} indicate the presence of C=O in amide group and 1062.78 cm^{-1} indicate the presence of C-O-C stretching of glycosides linkage and 893.04 cm^{-1} indicate the presence of –NH bending, respectively [26]. Appearance of new peaks at 1219.01 and 1018.41 cm^{-1} corresponds to P=O stretching, P-O stretching respectively was due to the interaction of sodium tripolyphosphate with chitosan and confirms the conversion of chitosan to nanochitosan.

The shift of the peaks observed at 3242.34 cm^{-1} to lower wave number in nanochitosan indicate cross linking had taken place effectively between sodium tripolyphosphate and chitosan. The characteristic peak for Zn–O group is located at 630.72 cm^{-1} is due to the attachment of amide group and stretching mode of ZnO [27]. In addition to these results, the characteristic peaks of (Fig. 2b) are shifted to lower wave number, the wide peak at 3454.75cm^{-1}, corresponding to the stretching vibration of hydroxyl, amino and amide groups, moved to lower wave numbers 3242.34 cm^{-1} and became broader and stronger, which indicated the strong interaction between these groups and ZnO [28] compared with (Fig. 2a), which could be explained in terms of strong attachment of ZnO to amide groups of chitosan molecules.

Thermal studies: Three weight loses were observed in the nanochitosan curve. TGA thermogram of nanochitosan as shown in Fig. 3a designated that the first thermal incident occurs at temperature range 50-150 ºC with a weight loss of 8% to 10%, which may be owing to the loss of residual water in the sample. The further weight loses at 300-400 ºC was due to the degradation of chitosan [29]. Nanochitosan starts by a disorderly splitting of the glycosidic bonds followed by a further decomposition to acetic, butyric and lower fatty acids. The second stage starts at the range of 170-370 ºC. The third stage starts at the range of 500-600 ºC. The thermal deprivation of nanochitosan upto 800 ºC shows that around 46.03% of sample remained as deposit at the end of the experiment shows high thermal stability of nanochitosan.

TGA thermogram of nanochitosan loaded ZnO designated that the first thermal decomposition occurs at temperature range 30-210 ºC with a weight loss from 8% to 9% is 18.24% which may be owing to the loss of residual water present in the sample (Fig. 3b). The second decomposition starts at 220 ºC and ends at 510 ºC. The weight loss is 29.51%, this may be owing to the thermal and oxidative decomposition of the sample [30]. The third stage of disintegration starts at 510 to 800 ºC. The weight loss is 2.277%. At end of the experiment nearly 49.90% of sample remained as deposit showing the higher thermal stability of nanochitosan encapsulated ZnO.

XRD studies: The XRD pattern of nanochitosan showed at 2θ = 18º and 20º. The XRD 2θ values at 10º and 20º of nanochitosan were disappeared or merged to give the broad peak at 18.86º during the formation of nanochitosan. The appearance of broad peak in nanochitosan may be due to the increase in packing of chitosan chains by the ionic crosslinking, which can deform the crystalline regions. In addition, the weakening of the rigid crystalline nature of chitosan after crosslinking may also be due to the disruption of NH_2 groups present in the glucosamine units in chitosan due to hydrogen bonding. These results indicated that an effective crosslinking, molecular miscibility and also certain interaction takes place between the chitosan with the ionic crosslinking agent. Thus, the XRD pattern of

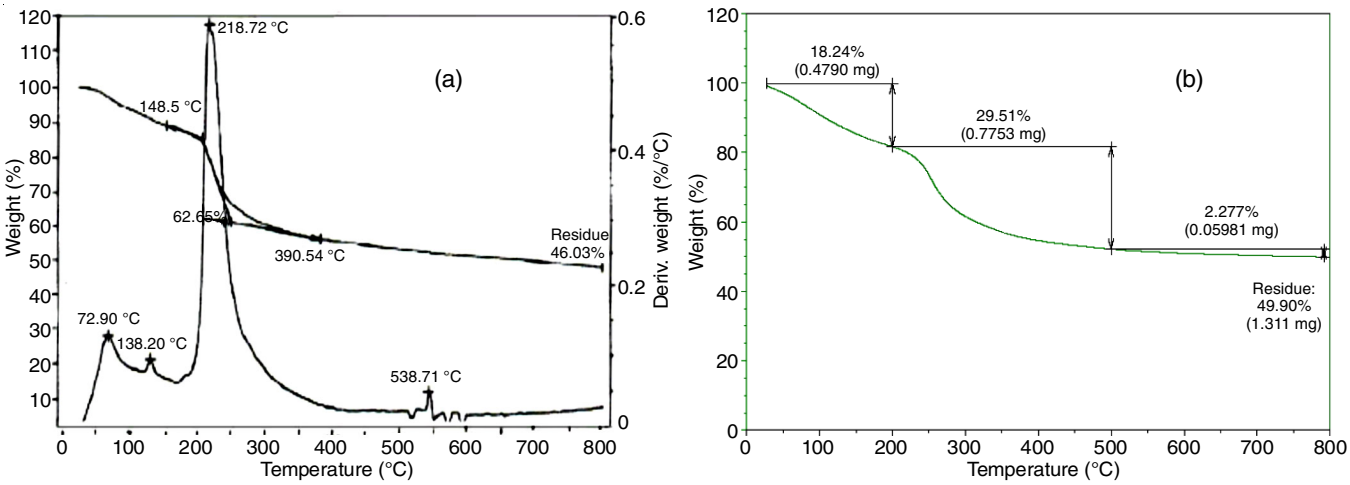

Fig. 3. TGA of (a) nanochitosan and (b) chitosan encapsulated ZnO nanoparticles

nanochitosan is a characteristic of an amorphous polymer [24]. The XRD patterns of nanochitosan showed a number of Bragg's diffraction peaks at 2θ of 21.38º, 23.80º, 26.47º and 51.35º. The average particle size of nanochitosan was calculated from four most intense peak using Debye-Scherrer's equation. The average particle size of nanochitosan was 24.7487 nm (Table-2).

TABLE-2
DETERMINATION OF THE AVERAGE PARTICLE SIZE OF THE NANOCHITOSAN

2θ (°)	FWHM (°)	B=π* FWHM/ 180 (radians)	D = Kλ/β cosθ (nm)
21.38	0.279	0.0048	30.0389
23.80	0.218	0.0038	34.0929
26.47	0.287	0.0050	23.3131
51.35	0.299	0.0052	11.5517
Average particle size			24.7487

The XRD spectra showed well defined distinctive peak at 2θ value of the broadening of peak was due to the amorphous, nature of chitosan/ZnO polymer by the ionic crosslinking at tripolyphosphate (TPP) with chitosan which can deform the crystalline structure of chitosan (Fig. 4b). The XRD patterns of chitosan encapsulated with ZnO nanoparticles showed a number of Bragg's diffraction peaks at 2θ of 28.20º, 36.21º, 39.72º, 49.12º, 53.58º, 56.40º. The average particle size of the chitosan/ZnO nanoparticles was calculated from the six most intense peak. The average particle size of chitosan encapsulated ZnO nanoparticles was 32.9757 nm (Table-3).

TABLE-3
DETERMINATION OF THE AVERAGE PARTICLE SIZE OF THE CHITOSAN ENCAPSULATED ZINC OXIDE NANOPARTICLES

2θ (°)	FWHM (°)	B=π* FWHM/ 180 (radians)	D = Kλ/β cosθ (nm)
28.20	0.0034	0.0479	32.1711
36.21	0.0017	0.0307	50.1954
39.72	0.0033	0.0655	23.5267
49.12	0.0030	0.0736	20.9375
53.58	0.0027	0.0723	21.3139
56.40	0.0011	0.0310	49.7096
Average particle size			32.9757

SEM studies: The SEM image was taken at different magnification including X 1,500, X 5000 and X 10,000 worked at 20 keV. Fig. 5 showed the SEM images of the synthesized chitosan nanoparticles. The images revealed the agglomerated nanoparticles having the size of nanoparticles in the range of 181 nm. If TPP concentration exceeds 1%, the chitosan aggregation was formed and precipitated, which might be due to more chitosan chains were crosslinked in the presence of high concentration of TPP. The diameter of chitosan-TPP nanoparticles increased with increase of TPP [31].

The surface morphology of chitosan encapsulated ZnO nanoparticles films was evaluated at different magnification

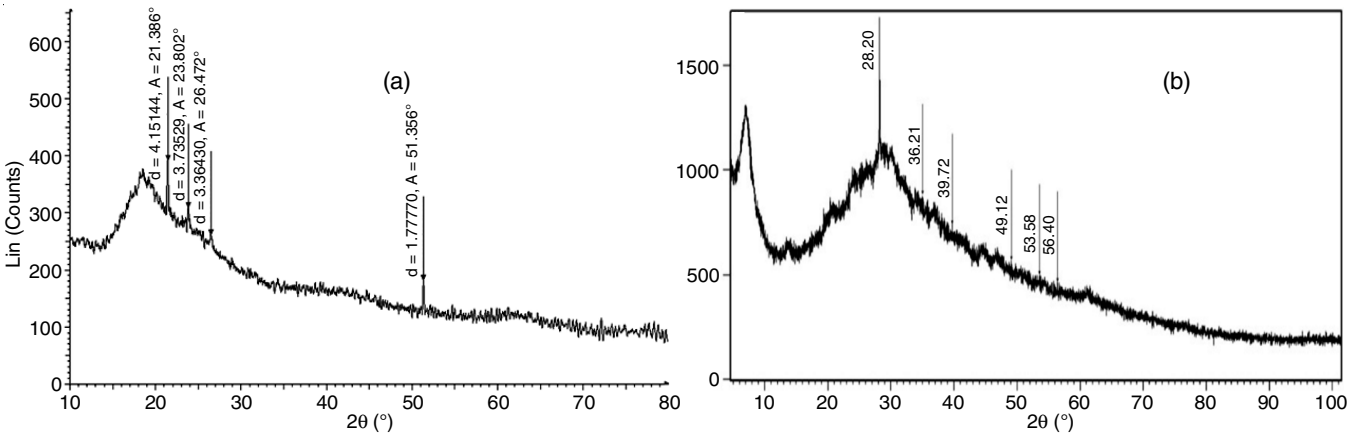

Fig. 4. XRD of (a) nanochitosan and (b) chitosan encapsulated ZnO nanoparticles

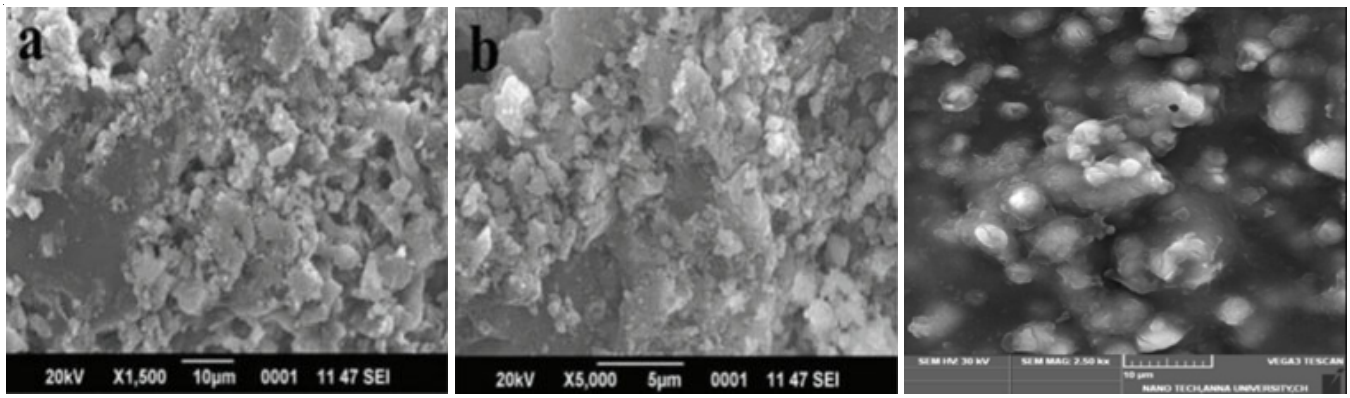

Fig. 5. SEM images of nanochitosan

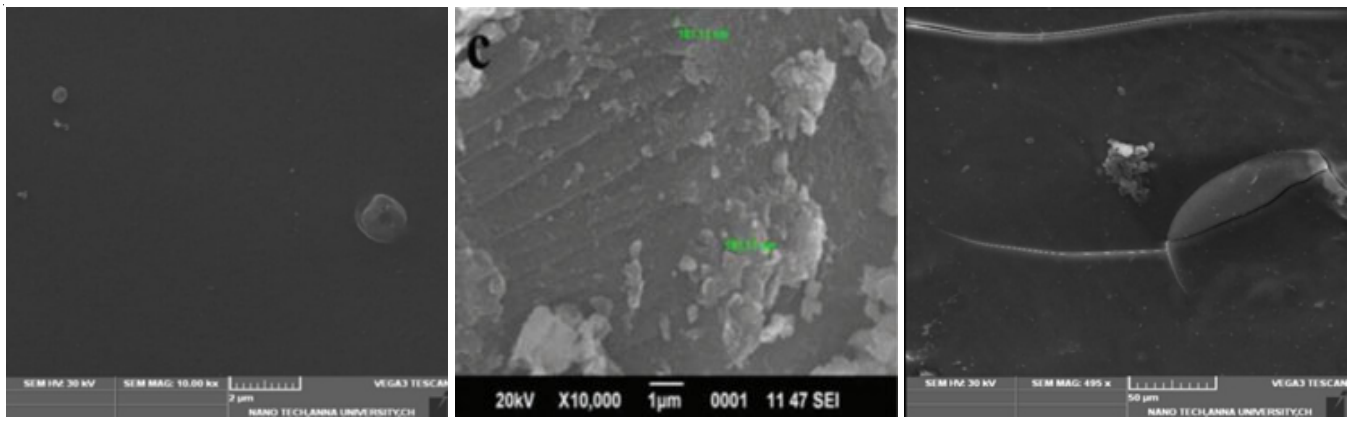

Fig. 6. SEM images of chitosan encapsulated ZnO nanoparticles

of 2000X, 10,000X and 50,000X. In the SEM photographs, presence of nanochitosan with ZnO nanoparticles on the polymer surface was spotted as white coloured images (Fig. 6). The surface of nanochitosan is film is rather smooth, compact and homogenous, whereas in films, the incorporation of nanoparticles (ZnO) modified the chitosan surface to coarse and heterogeneous.

Antimicrobial activity: The antibacterial activity of synthesized chitosan encapsulated ZnO nanoparticles was investigated against selected pathogens such as *S. aureus*, *E. coli*, *S. typhimurium* and *K. pneumonia* by using the agar well diffusion method and the results are shown in Table-4. In general, the synthesized of nanochitosan and chitosan encapsulated ZnO nanoparticles by using ionotropic gelation method exhibited strong antibacterial activity against Gram-negative bacteria (*E. coli* and *S. typhi*) and Gram-positive bacteria (*S. aureus*) bacteria strains. Similarly, the fungal strains such as *Aspergillus niger* and *Aspergillus flavus* were tested by agar well diffusion method and the results are shown in Table-5. Further, the result of antibacterial and antifungal activities clearly indicated that chitosan encapsulated ZnO nanoparticles in all concentration ranges showed a greater zone of inhibition against the studied bacterial and fungal strains compared to nanochitosan. This may be due to the small crystal size and the synergetic antibacterial activity of the chitosan encapsulated ZnO nanoparticles [32-34]. Ciprofloxacin was used as reference antibacterial agent. Furthermore, the chitosan encapsulated ZnO nanoparticles showed better antibacterial activity against Gram-positive and Gram-negative bacterial strains. Similarly, they also showed the better antifungal activity against *Aspergillus niger* and *Aspergillus flavus* as compared to amphotericin B as reference.

TABLE-4
ANTIBACTERIAL ACTIVITY OF CHITOSAN ENCAPSULATED ZINC OXIDE NANOPARTICLES

Microorganisms	Zone of inhibition (mm)			
	Control	R1	R2	Ciprofloxacin
Escherichia coli	–	10	17	18
Salmonella typhi	–	13	10	25
Klebsiella pneumonia	–	25	25	18
Enterococcus faecalis	–	12	10	30
Bacillus subtilis	–	12	13	30
Staphylococcus aureus	–	10	11	20

R1 = Nanochitosan; R2 = Chitosan encapsulated ZnO nanoparticles

TABLE-5
ANTIFUNGAL ACTIVITY OF CHITOSAN ENCAPSULATED ZINC OXIDE NANOPARTICLES

Microorganisms	Zone of inhibition (mm)			
	Control	R1	R2	Amphotericin-B
Candida albicans	–	12	11	15
Aspergillus niger	–	13	13	10
Aspergillus flavus	–	15	30	10

R1 = Nanochitosan; R2 = Chitosan encapsulated ZnO nanoparticles

Conclusion

In this study, nanochitosan and chitosan encapsulated zinc oxide nanoparticles were successfully synthesized and characterized by using ionotropic gelation method. From TGA analysis, the synthesized nanochitosan and chitosan encapsulated ZnO nanoparticles showed the thermal stability above 400 ºC. The crystallinity of the synthesized nanochitosan and chitosan encapsulated ZnO nanoparticles was evidenced from the XRD analysis and also showed an effective crosslinking, molecular miscibility and also certain interaction taken place between the chitosan with ionic crosslinking agent. The morphology of the synthesized nanochitosan and chitosan encapsulated ZnO nanoparticles were predominantly crystalline even though nanorod-shaped structures were also observed. Further, the synthesized nanochitosan and chitosan encapsulated ZnO nanoparticles have proved themselves to be strong antibacterial agent against *E. coli*, *S. typhi* and *S. aureus*. Similarly, effective antifungal activity against *A. niger* and *A. flavus* were also observed.

CONFLICT OF INTEREST

The authors declare that there is no conflict of interests regarding the publication of this article.

REFERENCES

1. L. Singh, H.G. Kruger, G.E.M. Maguire, T. Govender and R. Parboosing, *Ther. Adv. Infect. Dis.*, **4**, 105 (2017); https://doi.org/10.1177/2049936117713593
2. S.A. Agnihotri, N.N. Mallikarjuna and T.M. Aminabhavi, *J. Control. Release*, **100**, 5 (2004); https://doi.org/10.1016/j.jconrel.2004.08.010

3. K.M. Aiedeh, M.O. Taha and H. Al-Khatib, *J. Drug Deliv. Sci. Technol.*, **15**, 207 (2005); https://doi.org/10.1016/S1773-2247(05)50033-9
4. S.K. Shukla, A.K. Mishra, O.A. Arotiba and B.B. Mamba, *Int. J. Biol. Macromol.*, **59**, 46 (2013); https://doi.org/10.1016/j.ijbiomac.2013.04.043
5. J.H. Ryu, S. Hong and H. Lee, *Acta Biomater.*, **27**, 101 (2015); https://doi.org/10.1016/j.actbio.2015.08.043
6. F.J. Osonga, A. Akgul, I. Yazgan, A. Akgul, G.B. Eshun, L. Sakhaee and O.A. Sadik, *Molecules*, **25**, 2682 (2020); https://doi.org/10.3390/molecules25112682
7. M. Rai, A. Yadav and A. Gade, *Biotechnol. Adv.*, **27**, 76 (2009); https://doi.org/10.1016/j.biotechadv.2008.09.002
8. J. Sawai, *J. Microbiol. Methods*, **54**, 177 (2003); https://doi.org/10.1016/S0167-7012(03)00037-X
9. C.R. Mendes, G. Dilarri, C.F. Forsan, V.M.R. Sapata, P.R. Matos Lopes, P.B. de Moraes, R.N. Montagnolli, H. Ferreira and E.D. Bidoia, *Sci. Rep.*, **12**, 2658 (2022); https://doi.org/10.1038/s41598-022-06657-y
10. C.J. Frederickson, J.Y. Koh and A.I. Bush, *Nat. Rev. Neurosci.*, **6**, 449 (2005); https://doi.org/10.1038/nrn1671
11. S.A. Kelly, C.M. Havrilla, T.C. Brady, K.H. Abramo and E.D. Levin, *Environ. Health Perspect.*, **106**, 375 (1998); https://doi.org/10.1289/ehp.98106375
12. L.E. Rikans and K.R. Hornbrook, *Biochim. Biophys. Acta*, **1362**, 116 (1997); https://doi.org/10.1016/S0925-4439(97)00067-7
13. L. Zhang, Y. Jiang, Y. Ding, M. Povey and D. York, *J. Nanopart. Res.*, **9**, 479 (2007); https://doi.org/10.1007/s11051-006-9150-1
14. R. Brayner, R. Ferrari-Iliou, N. Brivois, S. Djediat, M.F. Benedetti and F. Fiévet, *Nano Lett.*, **6**, 866 (2006); https://doi.org/10.1021/nl052326h
15. P.K. Stoimenov, R.L. Klinger, G.L. Marchin and K.J. Klabunde, *Langmuir*, **18**, 6679 (2002); https://doi.org/10.1021/la0202374
16. T. Jayaramudu, K. Varaprasad, R.D. Pyarasani, K.K. Reddy, K.D. Kumar, A. Akbari-Fakhrabadi, R.V. Mangalaraja and J. Amalraj, *Int. J. Biol. Macromol.*, **128**, 499 (2019); https://doi.org/10.1016/j.ijbiomac.2019.01.145
17. E.M. Shapiro, *Magn. Reson. Med.*, **73**, 376 (2015); https://doi.org/10.1002/mrm.25263
18. V.K.H. Bui, D. Park, Y.-C. Lee, V. Gómez and S. Irusta, *Polymers*, **9**, 21 (2017); https://doi.org/10.3390/polym9010021
19. N. Othman, M.J. Masarudin, C.Y. Kuen, N.A. Dasuan, L.C. Abdullah and S.N.A.M. Jamil, *Nanomaterials*, **8**, 920 (2018); https://doi.org/10.3390/nano8110920
20. S. Logpriya, V. Bhuvaneshwari, D. Vaidehi, R.P. SenthilKumar, R.S. Nithya Malar, B.P. Sheetal, R. Amsaveni and M. Kalaiselvi, *J. Nanostruct. Chem.*, **8**, 301 (2018); https://doi.org/10.1007/s40097-018-0273-6
21. K.G.H. Desai, C. Liu and H.J. Park, *Microencapsulation*, **23**, 79 (2006); https://doi.org/10.1080/02652040500435360
22. K. Kataoka, T. Matsumoto, M. Yokoyama, T. Okano, S. Fukushima, Y. Sakurai, K. Okamoto and G.S. Kwon, *J. Control. Release*, **64**, 143 (2000); https://doi.org/10.1016/S0168-3659(99)00133-9
23. S. Bandara, C. Codi-anne, C. Johnson, F. Akindoju, E. Williams, J.M. Swaby, A. Oki and L.E. Carson, *Heliyon*, **4**, e00737 (2018); https://doi.org/10.1016/j.heliyon.2018.e00737
24. S. Vaezifar, S. Razavi, M.A. Golozar, S. Karbasi, M. Morshed and M. Kamali, *J. Cluster Sci.*, **24**, 891 (2013); https://doi.org/10.1007/s10876-013-0583-2
25. S.T. Lee, F.L. Mi, Y.J. Shen and S.S. Shyu, *Polymer*, **42**, 1879 (2001); https://doi.org/10.1016/S0032-3861(00)00402-X
26. K. Rajeshwari, S. Latha, T. Gomathi, K. Sangeetha and P.N. Sudha, *Der Pharm. Lett.*, **8**, 485 (2016).
27. G.-Y. Li, Y.-R. Jiang, K. Huang, P. Ding and J. Chen, *J. Alloys Compd.*, **466**, 451 (2008); https://doi.org/10.1016/j.jallcom.2007.11.100
28. M.M. Abd Elhady, *Int. J. Carbohydr. Chem.*, **2012**, 840591 (2012); https://doi.org/10.1155/2012/840591
29. S. Singh, D. Padovani, R.A. Leslie, T. Chiku and R. Banerjee, *J. Biol. Chem.*, **284**, 22457 (2009); https://doi.org/10.1074/jbc.M109.010868
30. E.B. Simsek, *J. Nat. Appl. Sci.*, **21**, 299 (2017); https://doi.org/10.19113/sdufbed.57694
31. J. Zhao and J. Wu, *Chin. J. Anal. Chem.*, **34**, 1555 (2006); https://doi.org/10.1016/S1872-2040(07)60015-2
32. C. Perez, M. Pauli and P. Bazerque, *Acta Biol. Med. Exp.*, **15**, 13 (1990).
33. N. Erdemoglu, E. Küpeli and E. Yesilada, *J. Ethnopharmacol.*, **89**, 123 (2003); https://doi.org/10.1016/S0378-8741(03)00282-4
34. C.F. Bagamboula, M. Uyttendaele and J. Debevere, *Food Microbiol.*, **21**, 33 (2004); https://doi.org/10.1016/S0740-0020(03)00046-7